# Identification and design of novel small molecule inhibitors against MERS-CoV papain-like protease via high-throughput screening and molecular modeling

Hyun Lee[*], Jinhong Ren, Russell P. Pesavento, Isabel Ojeda, Amy J. Rice, Haining Lv, Youngjin Kwon, Michael E. Johnson[*]

*Center for Biomolecular Sciences and Department of Medicinal Chemistry and Pharmacognosy, University of Illinois at Chicago, 900 S. Ashland, IL 60607, USA*

ABSTRACT

The development of new therapeutic agents against the coronavirus causing Middle East Respiratory Syndrome (MERS) is a continuing imperative. The initial MERS-CoV epidemic was contained entirely through public health measures, but episodic cases continue, as there are currently no therapeutic agents effective in the treatment of MERS-CoV, although multiple strategies have been proposed. In this study, we screened 30,000 compounds from three different compound libraries against one of the essential proteases, the papain-like protease (PL$^{pro}$), using a fluorescence-based enzymatic assay followed by surface plasmon resonance (SPR) direct binding analysis for hit confirmation. Mode of inhibition assays and competition SPR studies revealed two compounds to be competitive inhibitors. To improve upon the inhibitory activity of the best hit compounds, a small fragment library consisting of 352 fragments was screened in the presence of each hit compound, resulting in one fragment that enhanced the IC$_{50}$ value of the best hit compound by 3-fold. Molecular docking and MM/PBSA binding energy calculations were used to predict potential binding sites, providing insight for design and synthesis of next-generation compounds.

## 1. Introduction

The Middle East Respiratory Syndrome Coronavirus (MERS-CoV) was first documented in 2012 and has been found to be more challenging to control than the previously identified Severe Acute Respiratory Syndrome Coronavirus (SARS-CoV) that emerged nearly a decade earlier.[1] The history and current therapeutic options for both SARS and MERS, as well as the less severe infections by human coronavirus strains 229E, OC43, NL63 and HKU1 have recently been reviewed in detail.[2] Briefly, following its initial identification, MERS spread within the Middle East and beyond, with cases continuing to arise on a sporadic basis, particularly in Saudi Arabia and the United Arab Emirates.[3,4] There was also a major outbreak of MERS in South Korea in 2015. It was started from a returning traveler and spread through hospitals and infected a total of 186 people, 36 of which died.[5] Travel-related cases have been particularly challenging, as patients traveling from the Middle East present flu-like or pneumonia-like symptoms in other countries unprepared to recognize and treat MERS.[6]

As of January 2019, the WHO reported 2279 confirmed cases of MERS, resulting in 806 fatalities across 27 countries, with continuing reports of new episodic cases.[7] The mortality rate of MERS is 35.5%, which is much higher than was the case for SARS (approximately 10%). Camel to human transmission appears to be the primary source of infection,[8,9] with several studies implicating bats as the primary reservoir from which MERS-CoV originated.[10–12] Although an effective camel vaccine may ultimately be the best control strategy,[2,3] none appears likely in the near future. Person-to-person transmission occurs primarily from close contact in health-care settings or among stricken family members.[13,14] Although therapeutic options for the treatment of MERS-CoV infections have been the subject of recent reviews,[4,15,16] the continuing emergence of new cases of MERS-CoV combined with the high fatality rate and the potential for future viral mutation makes development of effective therapeutics a continuing priority.[1]

The multifunctional papain-like protease (PL$^{pro}$) isolated from MERS-CoV is recognized as a potentially druggable therapeutic target for the inhibition of viral replication.[17,18] In addition to a role in the

**Fig. 1.** High-throughput screening and hit confirmation. (A) Schematic of HTS and hit validation process. (B) Replicate plot from screening 30,000 compounds from Prestwick FDA-approved drugs, Maybridge and Chembridge libraries. The red box indicates hits with over 35% inhibition at 50 μM compound concentration.

selective cleavage of viral replicase polyproteins, MERS-Cov PL$^{pro}$ (MERS-PL$^{pro}$) has been shown to contribute to MERS-CoV pathogenicity *via* deISGylase and deubiquitinase activity on host proteins.[19,20] Recent studies further underscored the flexibility of MERS-PL$^{pro}$ when interacting with interferon stimulating gene product 15 (ISG15) from multiple species.[21] In this study, we identified new small molecule inhibitors of PL$^{pro}$ from high-throughput screening (HTS) of 30,000 compounds from three commercially available compound libraries including the FDA-approved drug library en route to potentially novel therapeutic alternatives in the future.

## 2. Results and discussion

### 2.1. High-throughput screening

A total of 30,000 compounds from three screening libraries (FDA-approved Prestwick, Maybridge and Chembridge libraries) were screened against MERS-PL$^{pro}$ by fluorescence intensity based enzymatic end-point assays followed by IC$_{50}$ value determination by dose-response. The overall systematic screening process is summarized in Fig. 1A, with compound numbers from each library listed in Table 1. The primary screens were done in duplicate using a Tecan liquid handling robot. The Z'-factors varied between 0.53 and 0.80 (average 0.67), indicating high quality of the screening campaign. The replicate plot of percent inhibition from duplicate data shown in Fig. 1B also illustrates the good quality of the screens. A total of 48 primary hit compounds exhibited greater than 35% inhibition at 50 μM compound concentration (shown in the red square in Fig. 1B). After careful examination of each hit compound structure, compounds that were either toxic or contained reactive functional groups were eliminated. Thirty compounds were cherry-picked and retested in triplicate for their percent inhibition by continuous enzymatic assays. Based upon

reproducible percent inhibition results, 23 compounds were selected and re-ordered from their commercial vendors for further hit validation.

### 2.2. HTS hit validation

The half maximal inhibitory concentration (IC$_{50}$) values were determined for 23 re-purchased compounds; dose-response curves of the two best compounds are shown in Fig. 2A. The IC$_{50}$ values in this work refer to the inhibition of the MERS-PL$^{pro}$ protease activity rather than inhibitory activity of MERS-CoV replication. The IC$_{50}$ values of compounds **1** and **6** were 25 μM and 20 μM, respectively. This reduced the number of hits to 12 compounds with IC$_{50}$ values below 55 μM. It is known that the enzymatic functional assay alone can be biased in selecting true positive hits. Consequently, the twelve selected compounds were subjected to a direct binding analysis with the MERS-PL$^{pro}$ enzyme by surface plasmon resonance (SPR) for further validation. The SPR sensorgrams of compound **6** at a series of increasing concentrations are shown in Fig. 2B as an example. Compound **6** possesses slow association and slow dissociation rates at $3.23 \times 10^3\, M^{-1}\, s^{-1}$ and $3.00 \times 10^{-2}\, s^{-1}$, respectively, resulting in a binding affinity (K$_D$) of 9.3 μM, and suggests that binding may be controlled through a gating mechanism. Of the initial 12 compounds, seven showed direct binding to the MERS-PL$^{pro}$ protein with a varying range of binding affinity (K$_D$) between 7.6 and 112 μM. Most of the seven compounds had K$_D$ values comparable to IC$_{50}$ values within 0.5 to 2-fold ranges (Fig. 2C). Of the seven validated hits, two compounds came out of a library of FDA-approved drugs, which are Pranlukast (compound **1**) and Sulfasalazine (compound **2**). Pranlukast is a cysteinyl leukotriene receptor-1 antagonist used for antagonism of bronchospasms caused by an allergic reaction to allergens in asthmatic patients and Sulfasalazine is being used to treat multiple diseases including rheumatoid arthritis, Crohn's

**Table 1**
Statistical parameters of all screened compounds from three libraries.

| Library | Number of compounds | Primary hits ≥35% inh | Reordered | IC$_{50}$ < 50 μM | Binding confirmed by SPR | Final hit rate[a] (%) |
|---|---|---|---|---|---|---|
| Prestwick | 1,200 | 17 | 7 | 4 | 2 | 0.167 |
| Maybridge | 14,400 | 11 | 6 | 3 | 2 | 0.014 |
| Chembridge | 14,400 | 20 | 10 | 5 | 3 | 0.021 |

[a] Final hit rates are calculated only for hits confirmed by SPR.
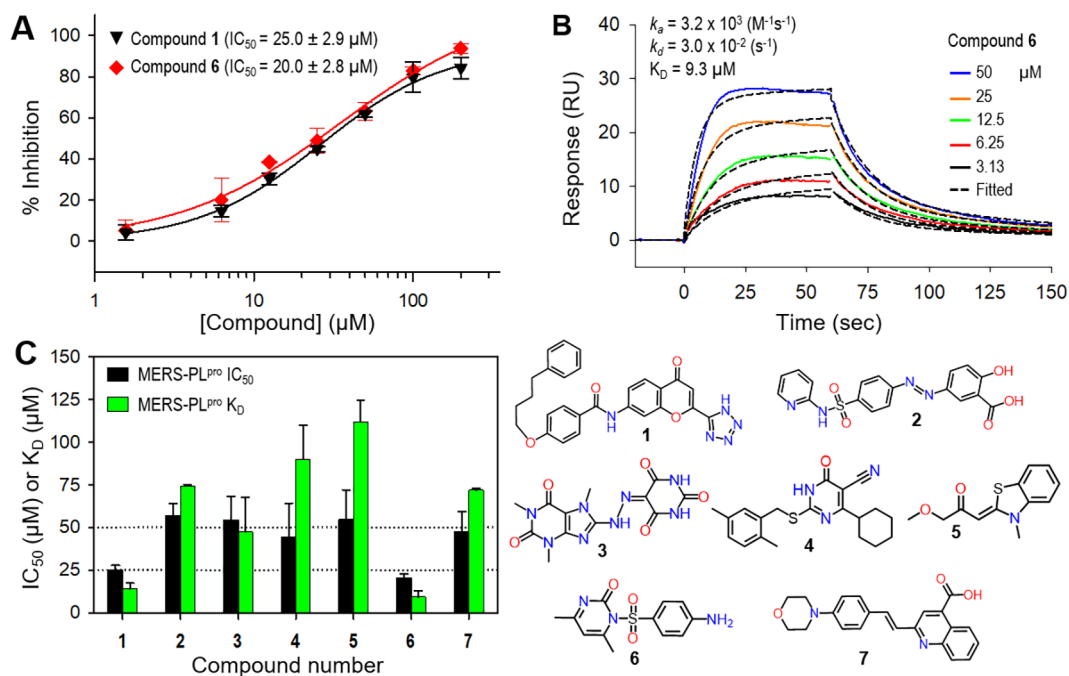
**Fig. 2.** Hit validation. (A) IC$_{50}$ fitting curve of compounds **1** and **6** using the Hill equation in SigmaPlot 12.0. IC$_{50}$ values of **1** and **6** were determined to be 25.0 μM and 20.0 μM, respectively. (The IC$_{50}$ values in this work refer to the inhibition of the MERS-PLpro protease activity rather than inhibitory activity of MERS-CoV replication.) (B) Sensorgrams of compound **6** at a series of increasing concentrations are shown in different colors. Black dotted lines are fitted curves from kinetics fitting using a 1:1 Langmuir binding model. (C) Bar graphs and structures of 7 selected compounds inhibitory activities (IC$_{50}$) and binding affinities (K$_D$) to MERS-PL$^{pro}$.

disease and ulcerative colitis. Two hits (compounds **3** & **4**) were from the diverse sets of the Maybridge library, and the Chembridge library produced three hits (compounds **5–7**).

### 2.3. Mechanism of inhibition and reversibility

To characterize potential mechanism of inhibition of the lead compounds (*i.e.*, **1**, **6**), enzymatic mode of inhibition studies were carried out varying both the inhibitor (0–200 μM) and substrate concentrations (100–300 μM). The best fit model was determined to be competitive inhibition for both compounds **1** and **6** with *K*i values of 127 μM and 36.6 μM, respectively (a Dixon plot of **6** is shown in Fig. 3A as an example). The IC$_{50}$ values of **1** and **6** were determined utilizing a fixed substrate concentration of 50 μM and remained similar at both 25 and 20 μM, differing significantly from the *K*i values listed above when both the substrate and inhibitor concentrations were varied, (Fig. 3B). It appears that compound **1** does not inhibit MERS-PL$^{pro}$ at higher substrate concentration. This may suggest that the substrate can compete out compound **1** easier than compound **6**, as confirmed by competition SPR. The K$_D$ values of compounds **1** and **6** alone were 14.1 μM and 7.6 μM. respectively. In the presence of 500 μM substrate, the binding of compound **1** was completely abolished, while that of compound **6** was 7-fold weaker (Fig. 3C). This indicates that the substrate competes with both compounds, with compound **1** more easily substituted by the substrate than compound **6**, in agreement with enzymatic assay results.

Both compounds **1** and **6** exhibited similar inhibitory activity and binding affinity to MERS-PL$^{pro}$; however, **6** is a more suitable lead candidate for further optimization because **6** has a lower molecular weight and also has a lower *K*i value than **1**. Hence, compound **6** was selected for further characterization, including reversibility studies. In addition to the observed dissociation in Fig. 2B, the reversibility of compound **6** was investigated via three different methods: dialysis, desalting and dilution. After complete inhibition of MERS-PL$^{pro}$ enzyme by compound **6**, both inhibited and control samples (DMSO) were dialyzed overnight in order to remove compound **6** and recover enzyme

activity. Unfortunately, the activity of the active enzyme control was completely lost after dialysis. Second, we utilized a desalting column to remove compound **6**, also resulting in the deactivation of active control sample. Thirdly, we set up both enzyme and compound **6** at very high concentrations and gradually diluted both active control and inhibited sample in the exact same manner and measured enzyme activity at each dilution step. If compound **6** behaves as an irreversible inhibitor, the enzyme activity should not recover once it is fully inhibited. (However deleted) The enzyme activity gradually recovered, providing support for compound **6** being a reversible inhibitor (Fig. 3D). The interaction between MERS-PL$^{pro}$ and compound **6** was also monitored by a 2D Transverse Relaxation Optimized Spectroscopy TROSY [$^1$H–$^{15}$N] NMR spectra using uniformly $^{15}$N-labeled His-tagged MERS-PL$^{pro}$ (Fig. 4). Although sequential assignment has not been carried out on apo-MERS-PL$^{pro}$, we observed more than thirteen peaks that either shifted (green dotted boxes with arrows) or disappeared (green solid boxes) upon compound **6** binding to MERS-PL$^{pro}$. The loss of $^1$H–$^{15}$N resonances may be attributed to either exchange broadening as compound **6** binds and dissociates or a conformational change in the MERS-PL$^{pro}$ backbone.

### 2.4. Preliminary structure-activity relationship (SAR)

The next step was to improve inhibitory activity of our lead compound **6**. We have searched analogs of **6**, but only the four analogs of compound **6** shown in Fig. 5A were commercially available. Based on activities of the five structural analogues, a preliminary structure-activity relationship (SAR) was obtained (Fig. 5B). The core functionality of our new lead scaffold is a benzene sulfonamide, and a separate six-membered nitrogen-containing ring is bound to the sulfonamide moiety at the R$^1$ location highlighted in blue. The pyrimidin-2 with two methyl groups at *ortho* and *para*-positions has better inhibitory activity (**6**, 73% inhibition) than piperazine-2,6-dione (**6a**, 16% inhibition) or piperidine (**6b**, 7% inhibition) moieties. However, it is unclear if either the methyl on the pyrimidin-2 or the heterocycle core itself is crucial for the maintenance of the activities. At the R$^2$ location shown in pink, the
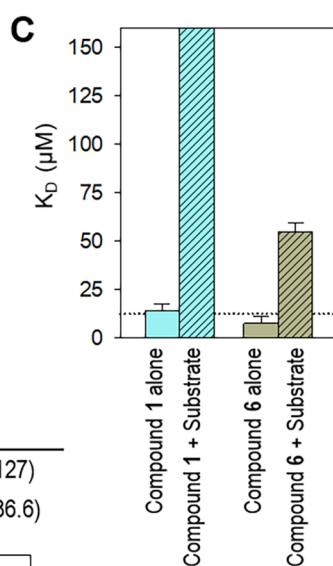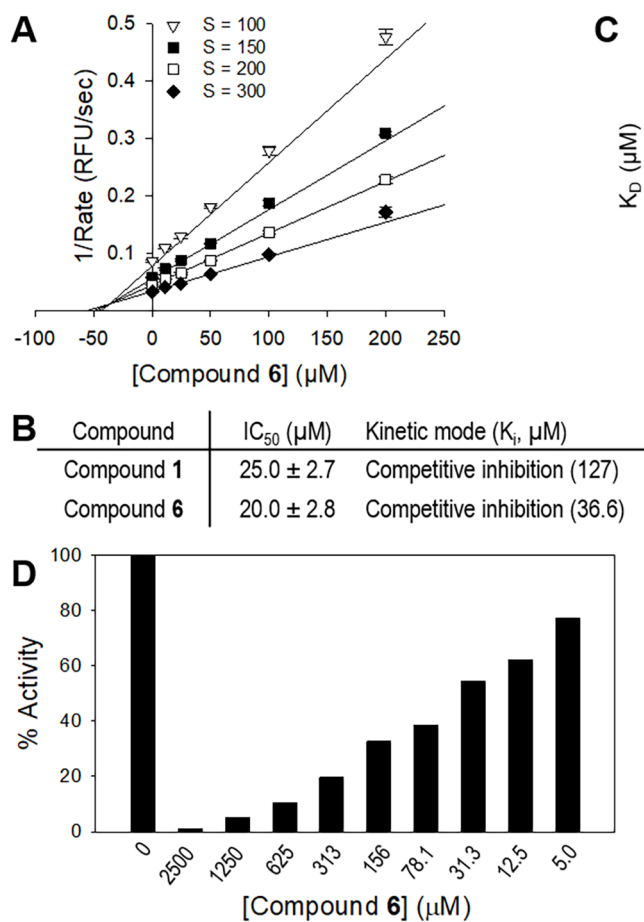
**Fig. 3.** Mechanism of inhibition. (A) Dixon plot for competitive inhibition of compound **6** ($Ki$ value of 36.6 μM). (B) Summary table of mechanism of inhibition of both compounds **1** and **6**. (C) Bar graphs of the dissociation equilibrium constants ($K_D$) of compounds **1** and **6** in the absence (solid bars) and in the presence (striped bars) of the substrate (Z-Arg-Leu-Arg-Gly-Gly-AMC). (D) Bar graphs of the enzyme activities of compound **6** to monitor reversibility.

| Compound | IC₅₀ (μM) | Kinetic mode (Kᵢ, μM) |
|---|---|---|
| Compound 1 | 25.0 ± 2.7 | Competitive inhibition (127) |
| Compound 6 | 20.0 ± 2.8 | Competitive inhibition (36.6) |
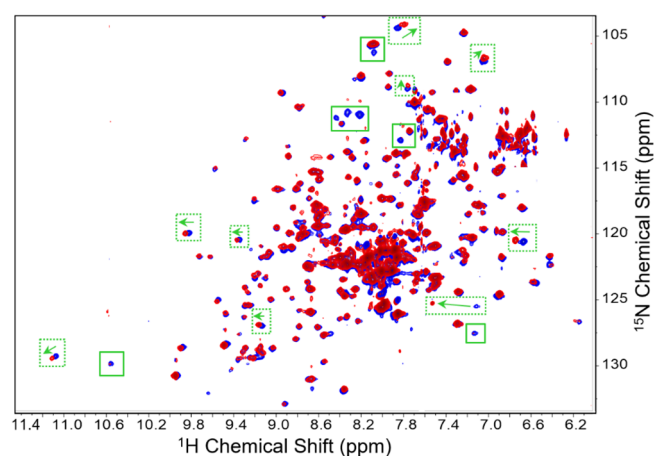


**Fig. 4.** 900 MHz TROSY [$^1$H–$^{15}$N] 2D NMR Spectra. Apo-MERS-PL$^{pro}$ (blue) and MERS-PL$^{pro}$ with excess amount of compound **6** (red) at pH 7.4. Peaks shifted are highlighted with green dotted boxes with arrows and peaks that disappeared upon compound **6** binding are boxed with solid green lines.

amino group at the *para*-position of benzene is essential for activity. When the amino group was replaced by methyl group (**6c**), the inhibitory activity decreased significantly to 11%, and the inhibitory activity was almost completely lost (2% inhibition) when the amino group was acetylated (**6d**). Given the limited number of structural analogs of **6**, the preliminary SAR simply underscores key structural features integral to the inhibitory activity.
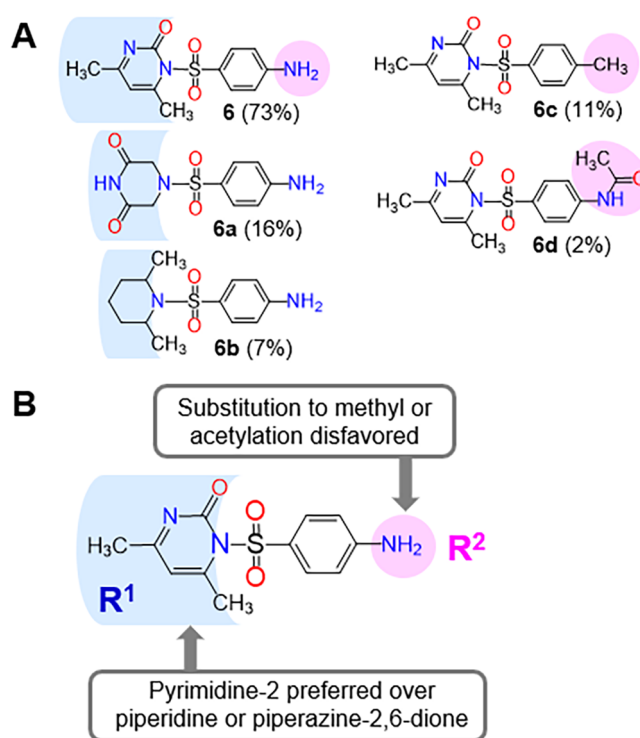


**Fig. 5.** Preliminary structure-activity relationship (SAR). (A) Structures of four analogs (**6a–6d**) of compound **6**. (B) Preliminary SAR map based on the five compounds.

**Table 2**
$IC_{50}$ value comparison of compound **6** in combination with fragment compounds from the Zenobia library.

| | Structure | $IC_{50}$ (µM) fragments | Compound 6 | |
|---|---|---|---|---|
| | | |  $IC_{50} = 20.0 \pm 2.8$ (µM) | |
| | | | $IC_{50}$ (µM) 6 + fragment | $IC_{50}$ Fold enhancement |
| ZT426 |  | $137 \pm 34$ | $14.6 \pm 4.2$ | 1.4 |
| ZT470 |  | $141 \pm 41$ | $15.4 \pm 3.6$ | 1.3 |
| ZT537 |  | $145 \pm 47$ | $10.9 \pm 8.2$ | 1.8 |
| ZT626 |  | $239 \pm 80$ | $6.6 \pm 1.9$ | 3.0 |
| ZT834 |  | $71.6 \pm 20.0$ | $11.1 \pm 3.2$ | 1.8 |

### 2.5. Zenobia fragment library screening in the presence of compound 6

None of the tested commercial analogs showed better inhibitory activity against MERS-PL^pro than the original lead compound **6**. This led us to screen a 352-compound Zenobia small fragment library in the presence of the lead compound **6** in an effort to increase inhibitory activity. The same fluorescence-base enzyme assay was used to screen the Zenobia library in attempts to search additional small fragments that can enhance inhibitory activity of **6**. Of the 352 fragment compounds, 11 fragments exhibited over 60% inhibition (> 10% inhibition enhancement) at 50 µM concentration in the presence of 20 µM compound **6**. Some fragments showed the opposite effect, decreasing the inhibitory activity of compound **6**, probably by competing for the same enzymatic binding site. Five fragments among the 11 selected fragments did improve the apparent $IC_{50}$ values of compound **6**, with improvements ranging from 1.3-fold to 3-fold better (Table 2). The $IC_{50}$ value of each fragment alone was also determined without compound **6** present, and they varied significantly between 71.6 µM (**ZT834**) and 239 µM (**ZT626**). Fragments **ZT426** and **ZT470** exhibited moderate enhancement with 1.3-fold and 1.4-fold improved $IC_{50}$ values for compound **6**, while another two fragments, **ZT537** and **ZT834**, enhanced the inhibitory activity of **6** slightly better, at almost 2-fold. Interestingly, the least effective fragment **ZT626** by itself had the best activity enhancement for compound **6**, reducing the $IC_{50}$ value by 3-fold to 6.6 µM. This suggests compound **6** and **ZT626** might inhibit MERS-PL^pro additively. In addition, the binding affinity of compound **6** in the presence of constant concentration of **ZT626** (200 µM) was determined to be similar (10.8 µM) to compound **6** alone (9.3 µM), suggesting that **ZT626** probably binds to a different location from the **6** binding site (Figs. 6 and 2B). Fig. 6A also shows that **ZT626** readily dissociates from MERS-PL^pro, indicating that its binding is also reversible.

### 2.6. Molecular docking and MD simulations

Compound **6** is a competitive inhibitor against MERS-PL^pro enzyme and competes with the substrate in the catalytic site. Molecular docking was performed for compound **6** in the catalytic site of MERS-PL^pro with GOLD5.2.2,[22] and three different binding poses for compound **6** were selected and shown in Fig. 7A. In order to investigate the most probable

binding pose, 5 ns molecular dynamic simulations were performed on the three conformations of compound **6** binding with MERS-PL^pro, followed by MM/PBSA binding affinity calculations using the AMBER14 package.[23] The calculated binding energies of the three binding poses ranged from –10.6 kcal mol$^{-1}$ to –15.8 kcal mol$^{-1}$ (Table 3). Pose 1 (shown in cyan in Fig. 7A) has the lowest calculated binding energy at –15.8 kcal mol$^{-1}$ among the three potential binding conformations and corresponds to relatively stable binding interactions. Therefore, pose 1 was selected as the most probable binding conformation for compound **6**.

Another round of molecular docking, MD simulations and MM/PBSA binding affinity calculations was carried out to predict the binding pose of the additive fragment **ZT626**. The docking of **ZT626** was performed in a 10 Å radius area around the compound **6** binding pose-1, keeping the position of compound **6** constant during fragment docking. Two different binding poses of **ZT626** were obtained from GOLD (Fig. 7B). Then 5 ns MD simulations and MM/PBSA calculations were performed on these ternary complexes (MERS-PL^pro/compound **6**/**ZT626**), using the same parameters as used for determination of binding poses for compound **6**. The binding energy of compound **6** was improved by the addition of **ZT626**/pose-1 to –17.4 kcal mol$^{-1}$ in comparison to compound **6** binding alone (–15.8 kcal mol$^{-1}$). On the other hand, the **ZT626** binding pose-2 showed an opposite effect, decreasing the overall binding energy to –13.8 kcal mol$^{-1}$. Therefore, pose-1 for **ZT626** was selected as the most probable binding conformation.

MM/PBSA binding energy calculations led us to choose pose-1 for both compound **6** and **ZT626** in MERS-PL^pro. The overall MERS-PL^pro enzyme structure and the potential binding poses of both compounds are shown in Fig. 8A. The carbonyl group of compound **6** could form an H-bond with the sidechain of Y279, and this residue could also form H-bonds with two phenolic hydroxyls of **ZT626** (pink circle in Fig. 8A). Hence, Y279 may play an important role for the binding of both compound **6** and **ZT626**. Meanwhile, the sidechain of S167 could also form an H-bond with one phenolic hydroxyl of the fragment compound. In addition, many hydrophobic interactions with the surrounding residues such as P163, D164, D165, G248, T249, P250, F269, E273, A275, V276, G277 and T308 are also important for the binding of compounds **6** and **ZT626** (Fig. 8B).

### 2.7. Fragment-merging and docking analyses

Based on the synergy effects for the fragment of **ZT626** with compound **6**, as well as their predicted binding conformations, we designed candidates with both structural moieties of **ZT626** and compound **6** via appropriate linkers for future synthesis. Our fragment-linking strategy involved in the replacement of sulfonyl group with chiral carbon to get the linking and extending position in compound **6**. Introducing a flexible linker with proper length is important for keeping the binding poses for both compound **6** and **ZT626**. Two atom, three atom and four atom linkers as alkyl or ester group between the newly introduced chiral carbon in compound **6** and the 3-hyroxy of **ZT626** were used. The molecular docking studies were carried out for these new compounds with different linkers to verify which structures recapitulate the key binding features of the compound **6** and fragment **ZT626**. From the molecular docking results, the two carbon linker (**L1**) appears inadequate for the proper binding of **ZT626** moiety (Fig. 9A). Therefore, we extended the linker to three or four atoms in compounds **L2** and **L3** (Fig. 9B & C), and the fragment moiety matches better than a two-carbon linker compound. This provides better direction for future compound synthesis, and also highlights interactions that contribute to inhibitor binding.

### 3. Conclusion

Although repurposing of HIV protease inhibitor, lopinavir/ritonavir,
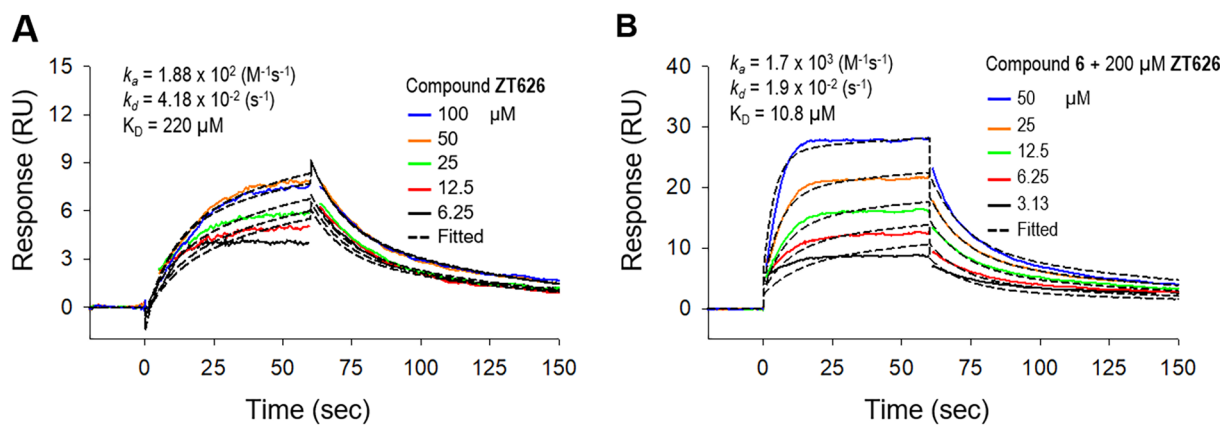
**Fig. 6.** Binding analysis by SPR. (A) Sensorgrams of compound **ZT626** at a series of increasing concentrations are shown in different colors. Black dotted lines are fitted curves from kinetics fitting using a 1:1 Langmuir binding model. (B) Sensorgrams of compound **6** at in the presence of 200 μM **ZT626**. Response of 200 μM **ZT626** was subtracted from each concentration of **6**.

has been found to be somewhat effective against MERS-CoV and could be a backup for the treatment of MERS, development of specific inhibitors targeting MERS-CoV are still needed.[5,26,27] We report a new small molecule scaffold effective as a competitive inhibitor against MERS-PL[pro]. This scaffold was identified from screening three structurally diverse compound libraries including the FDA-approved drug library called Prestwick. A thorough hit validation and confirmation strategy was applied, and produced two lead compounds with moderate inhibitory activity and binding affinity. These two compounds were characterized as competitive inhibitors based on both enzymatic mechanism of inhibition and competition SPR studies, one of which was selected as a better lead candidate for further characterization and development. Due to lack of commercially available analogs of lead compound **6**, only a very limited preliminary SAR was obtained. Hence, we explored a fragment-linking strategy to improve our lead compound activity. Additional small fragment library screening in the presence of the lead compound produced an additive fragment that can enhance the IC$_{50}$ value of the lead compound by 3-fold. Molecular docking and MM/ PBSA binding energy calculations were performed to predict the potential binding sites of compounds **6** and **ZT626**. This provides direction for the future design of fragment-linked inhibitors to improve its potency in developing inhibitors against MERS-PL[pro].

## 4. Materials and methods

### 4.1. Primary high-throughput screening

We screened three commercially available compound libraries purchased from the FDA-approved Prestwick, Maybridge, and Chembridge libraries, which consisted of 1200, 14,400 and 14,400 compounds, respectively. All compounds were dissolved in 100% DMSO and stored as 10 mM stock solutions in desiccated condition at −30 °C. The primary HTS assay was performed by a Tecan Freedom EVO 200 robot equipped with a Te-Mo 3 × 3 96-channel Liquid Handler dispenser and a 384-pin stainless steel pin tool (V&P Scientific) with a 200 nL capillary capacity. All assays were done in duplicate in black 384-well plates (Matrix Technologies) at room temperature. The MERS-PL[pro] enzyme was purified as described[28] and was prepared in assay buffer (50 mM HEPES, pH 7.5, 0.01% Triton X-100 (v/v), 0.1 mg mL$^{-1}$ BSA, and 2 mM DTT). 30 μL of enzyme solution (400 nM final concentration) was dispensed into wells, and then 200 nL of 10 mM compound (50 μM final concentrations) were added and incubated for 5 min. Enzyme reactions were initiated by adding 10 μL of substrate Z-Arg-Leu-Arg-Gly-Gly-AMC (Bachem Bioscience) at 50 μM final concentration dissolved in assay buffer and incubated for 6 min. Enzyme reactions were stopped by adding 10 μL of 10% SDS as a stop solution, and fluorescence intensity was monitored at 360 nm (excitation) and 450 nm (emission) with a Tecan Genios Pro microplate reader. Each plate contained a total of 32 positive and 32 negative controls.

### 4.2. Inhibitory activity (IC$_{50}$) value determination by dose response curve

Structures of the initial hit compounds from the HTS were examined, cherry-picked and reanalyzed by continuous kinetic assay by hand for confirmation. For those that showed over 50% inhibition at 50 μM concentration in the confirmation assay, IC$_{50}$ values were measured using the same assay conditions as the primary screen by hand in
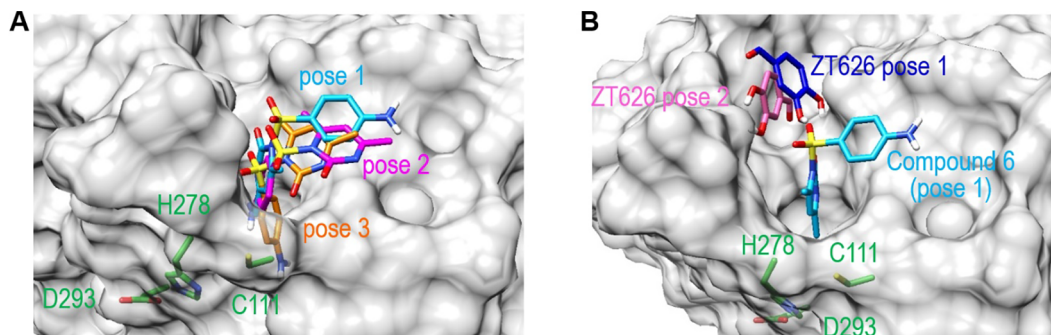


**Fig. 7.** Molecular docking for compound **6** and **ZT626**. (A) The three predicted binding poses of compound **6** (pose-1: colored in cyan; pose-2: colored in magenta; pose-3: colored in orange) with MERS-PL[pro]. (B) The two possible binding poses of fragment **ZT626** (pose-1: colored in dark blue; pose-2: colored in pink) with the pose-1 binding position of compound **6** in MERS-PL[pro]. The pictures of binding modes of compound **6** and **ZT626** with MERS-PL[pro] were made from Chimera1.10.2.[24] Catalytic residues of C111, H278, and D293 are colored in green with only sidechains shown.

**Table 3**
The energy components for binding affinity of ΔH of compound **6** with MERS-PL$^{pro}$ by MM/PBSA calculation.

| | $\Delta E_{vdW}$[a] (kcal mol$^{-1}$) | $\Delta E_{ele}$[b] (kcal mol$^{-1}$) | $\Delta G_{pol}$[c] (kcal mol$^{-1}$) | $\Delta G_{nonpol}$[d] (kcal mol$^{-1}$) | $\Delta H_{bind}$[e] (kcal mol$^{-1}$) |
|---|---|---|---|---|---|
| Compd **6** Pose 1 alone | $-28.4 \pm 3.3$ | $-8.4 \pm 6.7$ | $23.7 \pm 5.9$ | $-2.6 \pm 0.2$ | $-15.8 \pm 3.0$ |
| Compd **6** Pose 2 alone | $-19.4 \pm 2.4$ | $-11.8 \pm 5.1$ | $20.6 \pm 4.4$ | $-2.0 \pm 0.2$ | $-12.5 \pm 4.0$ |
| Compd **6** Pose 3 alone | $-17.7 \pm 3.5$ | $-17.2 \pm 9.6$ | $26.4 \pm 6.8$ | $-2.1 \pm 0.2$ | $-10.6 \pm 6.5$ |
| Compd **6** Pose 1 + **ZT626** Pose 1 | $-29.0 \pm 3.1$ | $-20.3 \pm 5.9$ | $34.8 \pm 4.9$ | $-2.9 \pm 0.1$ | $-17.4 \pm 3.0$ |
| Compd **6** Pose 1 + **ZT626** Pose 2 | $-28.1 \pm 3.2$ | $-6.8 \pm 8.1$ | $23.7 \pm 7.3$ | $-2.7 \pm 0.2$ | $-13.8 \pm 3.5$ |

[a] van der Waals contribution.
[b] Electrostatic energy.
[c] Polar solvation free energy.
[d] Nonpolar solvation free energy.
[e] Binding enthalpy. The data are shown in average ± SD.

triplicate. A series of increasing concentrations (0–200 μM final concentration at 2-fold serial dilution) in 100% DMSO were prepared in a 384-well plate. 7 μL of 600 nM (3X) enzyme solution was distributed into wells, and 7 μL of varying concentration of 3X compounds were added and incubated for 5 min. The enzyme reaction was initiated by adding 7 μL of the 150 μM (3X) substrate, and its activity was continuously monitored for at least 10 min. The IC$_{50}$ values were calculated by fitting the data with the Hill equation (1), using SigmaPlot v12.0 where $y$ is percent inhibition, $x$ is inhibitor concentration, $n$ is the slope of the concentration–response curve (Hill slope), and $V_{max}$ is maximal inhibition from three to four independent assays.

$$y = V_{max}\left(\frac{x^n}{IC_{50}^n + x^n}\right) \tag{1}$$

### 4.3. Determination of dissociation equilibrium constant ($K_D$) by SPR

The MERS-PL$^{pro}$ enzyme was diluted to 50 μg/mL with 10 mM sodium acetate (pH 5.5) and immobilized on a CM5 sensor chip by standard amine-coupling with running buffer PBSP (10 mM phosphate, pH 7.4, 2.7 mM KCl, 137 mM NaCl, 0.05% surfactant P-20) using a Biacore T200 instrument. MERS-PL$^{pro}$ enzyme was immobilized to flow cells 2 and 4, and immobilization levels were ~10,000 RU for both flow cells. Unmodified flow cells 1 and 3 were used as controls. Compound solutions with a series of increasing concentrations (0–50 μM at 2-fold dilution) were applied to all four channels in SPR binding buffer (PBSP + 0.5 mM TCEP and 2% DMSO) at a 30 μL/min flow rate at 25 °C. Data were double-referenced with both reference cell RU values and zero concentration (2% DMSO) signals, and sensorgrams were

analyzed using the Biacore T200 evaluation software 3.0. Response units at each concentration were measured during the equilibration phase for steady-state affinity fittings, and the K$_D$ values were determined by fitting the data to a single rectangular hyperbolic curve Eq. (2), where $y$ is the response, $y_{max}$ is the maximum response and $x$ is the compound concentration.

$$y = \frac{y_{max}\cdot x}{K_D + x} \tag{2}$$

Kinetic rate constants were determined by fitting globally to the 1:1 Langmuir model embedded in the Biacore T200 evaluation software v3.0.

### 4.4. Mechanism of inhibition

Enzymatic activities of MERS-PL$^{pro}$ were investigated in the same way as the IC$_{50}$ value determination by varying concentration of both substrate (0–300 μM) and inhibitors (0–200 μM). The data were fit to four equations (3–6) using SigmaPlot Enzyme Kinetics Module 1.3 in order to determine the best fit inhibition mechanism and kinetic parameters for each compound.

$$\text{Competitive inhibition} \quad v = \frac{v_{max}}{\left(1 + \frac{k_m}{[S]}\right)\left(1 + \frac{[I]}{K_i}\right)} \tag{3}$$

$$\text{Non - competitive inhibition} \quad v = \frac{v_{max}}{\left(1 + \frac{[I]}{k_i}\right)\left(1 + \frac{k_m}{[S]}\right)} \tag{4}$$
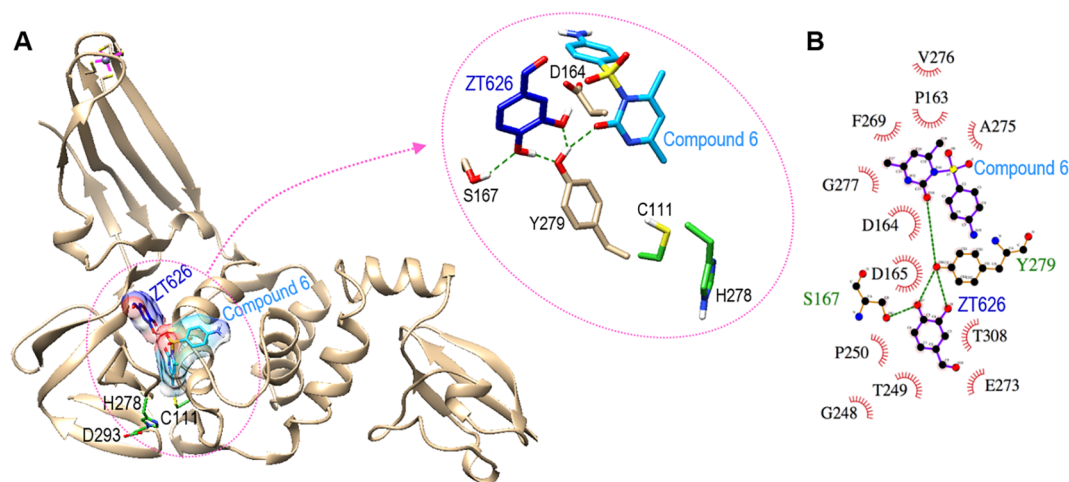


**Fig. 8.** Docking pose of compound 6 and a fragment ZT626. (A) Predicted conformation of compound **6** in the active site of MERS-PL$^{pro}$ with an enlarged figure presenting interactions in detail shown in pink circle. (B) The interactions of compound **6** and **ZT626** in MERS-PL$^{pro}$ with H-bonds shown in green dash lines and van der Waals in red lines by LigPlot$^+$.[25]
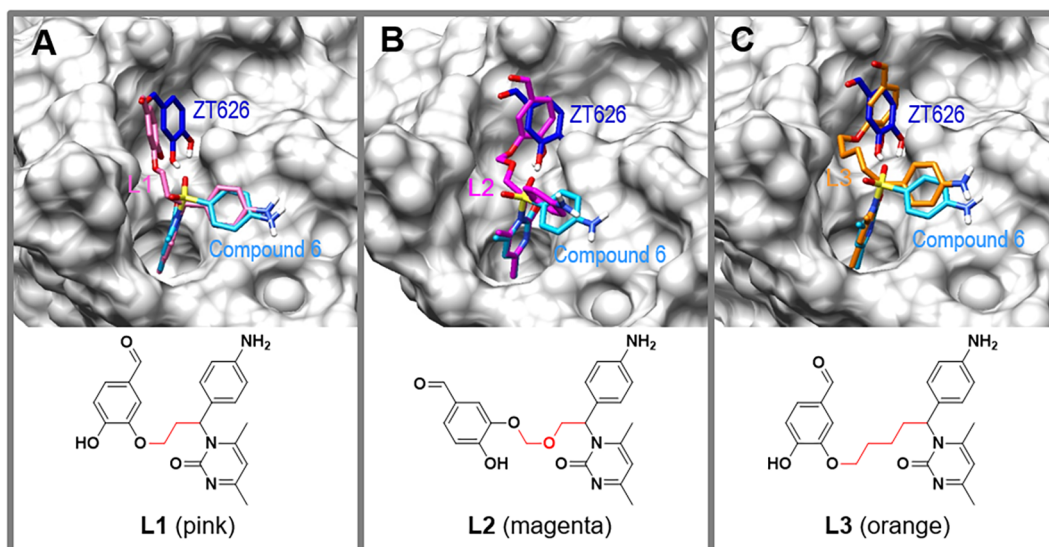
**Fig. 9.** The designed compounds from fragment linking strategy and their predicted binding poses. Among three designed compounds for synthesis, two compounds (**L2** and **L3**) nearly recapitulate the binding pose of compound **6** and **ZT626** after molecular docking. The linkers were colored in red in the structures. Compound **6** is colored in sky blue, **ZT626** is colored in dark blue and the MERS-PL$^{pro}$ enzyme is shown in grey surface.

Uncompetitive inhibition

$$v = \frac{v_{\max}}{1 + \frac{[I]}{K_i} + \frac{K_m}{[S]}} \quad (5)$$

Mixed - type inhibition

$$v = \frac{v_{\max}}{\left(\frac{K_m}{[s]}\right)\left(1 + \frac{[I]}{K_i}\right) + \left(1 + \frac{[I]}{\alpha K_i}\right)} \quad (6)$$

where $V$ is the reaction rate, $V_{max}$ is the maximum rate of the reaction, $K_m$ is the Michaelis-Menten constant for the substrate, $[S]$ is the substrate concentration, $[I]$ is the inhibitor concentration, $K_i$ is the dissociation constant of the inhibitor I to the free enzyme and $\alpha K_i$ is the dissociation constant for the inhibitor I to the ES complex.

### 4.5. Reversibility of inhibition

4 µM MERS-PL$^{pro}$ was incubated with compound **6** at 125X the concentration of the IC$_{50}$ for 1 h at room temperature in assay buffer containing 50 mM HEPES (pH 7.5), 2 mM DTT, 0.1 mg/ml BSA, and 0.01% Triton X-100 in a final volume of 200 µL. Control MERS-PL$^{pro}$ without any compound was also prepared in the same way with the same volume of DMSO. Then, both samples were diluted by 2-fold using assay buffer (Supplementary Fig. S1). MERS-PL$^{pro}$ enzyme activity of both samples were measured. Seven additional 2-fold dilutions were done followed by enzyme activity measurement. MERS-PL$^{pro}$ activity was measured in the same way as IC$_{50}$ measurements.

### 4.6. Zenobia fragment library screening

The Zenobia fragment library consisting of 352 compounds was screened in a similar way as the primary HTS. The original stock concentration of all fragments was 200 mM dissolved in 100% DMSO and they were diluted do 20 mM in 100% DMSO. Compound **6** was added to assay buffer at 20 µM final concentration for screening wells, and 16 positive and 16 negative controls contained the same amount of just DMSO. 30 µL of enzyme solution (400 nM final concentration) was dispensed into wells, and then 200 nL of 20 mM fragment (100 µM final concentrations) were added and incubated for 5 min. Enzyme reactions were initiated with 10 µL of substrate (50 µM final concentration) dissolved in assay buffer and incubated for 6 min. Enzyme reactions were continuously monitored for 10 min at 360 nm (excitation) and 450 nm (emission) with a Tecan Genios Pro microplate reader.

### 4.7. Molecular docking and MD simulations for compound 6

The crystal structure of the MERS-PL$^{pro}$ in complex with ubiquitin (PDB code 4RF1[29] with resolution of 2.15 Å) was selected to perform molecular docking. The MERS-PL$^{pro}$ structure was optimized through the Protein Preparation Wizard in the Schrödinger Suite.[30] All hydrogens and charges were added in the OPLS3 force field. Restrained minimization was performed on the added hydrogens. Meanwhile, the LigPrep module in the Schrödinger Suite[31] was used to create the 3D structures of compound **6** as well as to perform the geometric optimization. Molecular docking was performed by GOLD v5.2.2[22] using the above prepared MERS-PL$^{pro}$ and compound **6**. Ubiquitin was extracted before performing docking, and the active site for MERS-PL$^{pro}$ was defined as being within a 10 Å radius around the catalytic residue Cys111 for the docking of compound **6**. The MERS-PL$^{pro}$ was maintained static, while compound **6** was flexible with "flip amide bonds", "detect internal H bonds", and "flip ring corners" set to on during ligand conformations searching. Other parameters applied default values in GOLD. Then three different binding poses for compound **6** were chosen for the following MD simulations and subsequent MM/PBSA calculation to predict binding affinities using the AMBER14 suite of programs.[23] Preparation of the MD simulations included assigning Restrained Electrostatic Potential (RESP) atomic partial charges to compound **6** using HF/6-31G* and Gaussian 09 in the R.E.D. online server,[32] and then assigning the general AMBER force field[33] (GAFF) parameters to the above prepared ligand. A 10 Å octahedral TIP3P water molecule box was added to each of the complex systems using Cl$^-$ counter-ions to neutralize the system. The Amber FF14SB force field was applied for the system. The systems were first minimized using 10,000 steps of steepest descent minimization followed by another 10,000 steps of conjugate gradient minimization. After heating from 0 K to 300 K over 100 ps, the systems were equilibrated over 100 ps at constant pressure (1 bar) and temperature (300 K) with a restraint of 10 kcal mol$^{-1}$ Å$^{-2}$ on the complex and then subsequently without any restraint. Then 5 ns NPT production runs without positional restraints were performed at 300 K and 1 bar for the systems. The atomic coordinates were saved every 2.5 ps. During the MD simulation, all bonds involving hydrogen atoms were constrained to their equilibrium distance using the SHAKE algorithm,[34] and a time step of 2 fs. The python script, MMPBSA.py,[35] included in AMBER 14, was used to perform the MM/PBSA calculations using the 1200 frames from the last 3 ns of the 5 ns simulation

trajectory file. Default parameters were applied in binding affinity calculations.

### 4.8. Molecular docking and MD simulations for the fragment of ZT626

The binding site for the fragment of **ZT626** was selected as being 10 Å around the above predicted binding position of compound **6**. After docking, two different binding poses of **ZT626** were picked to perform the subsequent 5 ns MD simulations and the binding energy calculation for compound **6**. Consistent parameters were applied to MD simulations for the ternary complexes of MERS-PL^pro/compound **6**/**ZT626** and that of the binary complex of MERS-PL^pro/compound **6**, in order to compare the binding affinity difference for compound **6** by incorporating **ZT626**.

### 4.9. 900 MHz TROSY [$^1$H–$^{15}$N] 2D NMR spectra

2D NMR spectra of uniformly $^{15}$N-labeled His-tagged Apo-MERS-PL$^{pro}$, in the presence and absence of excess compound **6**, were recorded on a Bruker 900 MHz NMR spectrometer. Each NMR solution contained $^{15}$N-labeled HIS-tagged MERS-PL$^{pro}$ (240 μM), 25 mM KH$_2$PO$_4$ (pH 7.4), 25 mM KCl, 1 mM DTT and 10% D$_2$O. The MERS-PL$^{pro}$ + excess inhibitor spectrum was generated by adding four equivalents of compound **6** (in $d^6$-DMSO) to Apo-MERS-PL$^{pro}$, producing an aqueous buffer with 3% DMSO. Each solution was gently vortexed, transferred to a 5 mm OD 7″L glass NMR tube, and the Transverse Relaxation Optimized Spectroscopy TROSY [$^1$H–$^{15}$N] spectrum was acquired overnight at RT. SPARKY was utilized to process the NMR data and produce the images.

### Author contributions

HL performed all experiments with assistance of AJR, IO, HLv and YK. JR performed computational studies. RPP did 2D NMR studies. HL, JR, RPP and MEJ designed the experiments and wrote the manuscript.

### Appendix A. Supplementary data

Supplementary data to this article can be found online at https://doi.org/10.1016/j.bmc.2019.03.050.

### References

1. Chafekar A, Fielding BC. MERS-CoV: understanding the latest human coronavirus threat. *Viruses.* 2018;10(2).
2. Zumla A, Chan JF, Azhar EI, Hui DS, Yuen KY. Coronaviruses – drug discovery and therapeutic options. *Nat Rev Drug Discovery.* 2016;15(5):327–347.
3. Chan JF, Lau SK, To KK, Cheng VC, Woo PC, Yuen KY. Middle East respiratory syndrome coronavirus: another zoonotic betacoronavirus causing SARS-like disease. *Clin Microbiol Rev.* 2015;28(2):465–522.
4. Al-Tawfiq JA, Memish ZA. Update on therapeutic options for middle east respiratory syndrome coronavirus (MERS-CoV). *Expert Rev Anti Infect Ther.* 2017;15(3):269–275.
5. Kim UJ, Won EJ, Kee SJ, Jung SI, Jang HC. Combination therapy with lopinavir/ritonavir, ribavirin and interferon-alpha for Middle East respiratory syndrome. *Antivir Ther.* 2016;21(5):455–459.
6. Hui DS, Perlman S, Zumla A. Spread of MERS to South Korea and China. *Lancet Respir Med.* 2015;3(7):509–510.
7. World-Health-Organization. Middle East Respiratory Syndrome Coronavirus (MERS-CoV); http://www.who.int/emergencies/mers-cov/en/ [accessed 20 September 2016].
8. Haagmans BL, Al Dhahiry SH, Reusken CB, et al. Middle East respiratory syndrome coronavirus in dromedary camels: an outbreak investigation. *Lancet Infect Dis.* 2014;14(2):140–145.
9. Reusken CB, Haagmans BL, Muller MA, et al. Middle East respiratory syndrome coronavirus neutralising serum antibodies in dromedary camels: a comparative serological study. *Lancet Infect Dis.* 2013;13(10):859–866.
10. Corman VM, Ithete NL, Richards LR, et al. Rooting the phylogenetic tree of middle East respiratory syndrome coronavirus by characterization of a conspecific virus from an African bat. *J Virol.* 2014;88(19):11297–11303.
11. Lau SK, Li KS, Tsang AK, et al. Genetic characterization of Betacoronavirus lineage C viruses in bats reveals marked sequence divergence in the spike protein of pipistrellus bat coronavirus HKU5 in Japanese pipistrelle: implications for the origin of the novel Middle East respiratory syndrome coronavirus. *J Virol.* 2013;87(15):8638–8650.
12. Wang Q, Qi J, Yuan Y, et al. Bat origins of MERS-CoV supported by bat coronavirus HKU4 usage of human receptor CD26. *Cell Host Microbe.* 2014;16(3):328–337.
13. Al-Abdallat MM, Payne DC, Alqasrawi S, et al. Hospital-associated outbreak of Middle East respiratory syndrome coronavirus: a serologic, epidemiologic, and clinical description. *Clin Infect Dis.* 2014;59(9):1225–1233.
14. Assiri A, McGeer A, Perl TM, et al. Hospital outbreak of Middle East respiratory syndrome coronavirus. *N Engl J Med.* 2013;369(5):407–416.
15. Zhou Y, Yang Y, Huang J, Jiang S, Du L. Advances in MERS-CoV vaccines and therapeutics based on the receptor-binding domain. *Viruses.* 2019;11(1).
16. Liang R, Wang L, Zhang N, et al. Development of small-molecule MERS-CoV inhibitors. *Viruses.* 2018;10:12.
17. Lei J, Mesters JR, Drosten C, Anemuller S, Ma Q, Hilgenfeld R. Crystal structure of the papain-like protease of MERS coronavirus reveals unusual, potentially druggable active-site features. *Antiviral Res.* 2014;109:72–82.
18. Yang L, Wu Z, Ren X, et al. MERS-related betacoronavirus in Vespertilio superans bats, China. *Emerg Infect Dis.* 2014;20(7):1260–1262.
19. Daczkowski CM, Goodwin OY, Dzimianski JV, Farhat JJ, Pegan SD. Structurally guided removal of DeISGylase biochemical activity from papain-like protease originating from middle east respiratory syndrome coronavirus. *J Virol.* 2017;91(23).
20. Mielech AM, Kilianski A, Baez-Santos YM, Mesecar AD, Baker SC. MERS-CoV papain-like protease has deISGylating and deubiquitinating activities. *Virology.* 2014;450–451:64–70.
21. Daczkowski CM, Dzimianski JV, Clasman JR, Goodwin O, Mesecar AD, Pegan SD. Structural Insights into the interaction of coronavirus papain-like proteases and interferon-stimulated gene product 15 from different species. *J Mol Biol.* 2017;429(11):1661–1683.
22. Verdonk ML, Cole JC, Hartshorn MJ, Murray CW, Taylor RD. Improved protein–ligand docking using GOLD. *Proteins Struct Funct Bioinf.* 2003;52(4):609–623.
23. Case DA, Babin V, Berryman JT, et al. {Amber 14}; 2014.
24. Pettersen EF, Goddard TD, Huang CC, et al. UCSF Chimera—a visualization system for exploratory research and analysis. *J Comput Chem.* 2004;25(13):1605–1612.
25. Laskowski RA, Swindells MB. LigPlot +: multiple ligand-protein interaction diagrams for drug discovery. *J Chem Inf Model.* 2011;51(10):2778–2786.
26. Arabi YM, Alothman A, Balkhy HH, et al. Treatment of middle east respiratory syndrome with a combination of lopinavir-ritonavir and interferon-β1b (MIRACLE trial): study protocol for a randomized controlled trial. *Trials.* 2018;19(1):81.
27. Chen H, Chan JF-W, Yuen Treatment K-Y, et al. With lopinavir/ritonavir or interferon-β1b improves outcome of MERS-CoV infection in a nonhuman primate model of common marmoset. *J Infect Dis.* 2015;212(12):1904–1913.
28. Lee H, Lei H, Santarsiero BD, et al. Inhibitor recognition specificity of MERS-CoV papain-like protease may differ from that of SARS-CoV. *ACS Chem Biol.* 2015;10(6):1456–1465.
29. Bailey-Elkin BA, Knaap RCM, Johnson GG, et al. Crystal structure of the middle east respiratory syndrome coronavirus (MERS-CoV) papain-like protease bound to ubiquitin facilitates targeted disruption of deubiquitinating activity to demonstrate its role in innate immune suppression. *J Biol Chem.* 2014;289(50):34667–34682.
30. Schrödinger Release 2016-1: Schrödinger Suite 2016-1 Protein Preparation Wizard; Epik Version 3.5, Schrödinger, LLC, New York, NY; Impact version 7.0, Schrödinger, LLC, New York, NY; Prime version 4.3, Schrödinger, LLC, New York, NY; 2016.
31. Schrödinger Release 2016-1: Ligprep, Version 3.7. Schrödinger, LLC: New York, NY; 2016.
32. Vanquelef E, Simon S, Marquant G, Server RED, et al. a web service for deriving RESP and ESP charges and building force field libraries for new molecules and molecular fragments. *Nucleic Acids Res.* 2011;39(Suppl_2):W511–W517.
33. Wang JM, Wolf RM, Caldwell JW, Kollman PA, Case DA. Development and testing of a general amber force field. *J Comput Chem.* 2004;25(9):1157–1174.
34. Kräutler V, van Gunsteren WF, Hünenberger PH. A fast SHAKE algorithm to solve distance constraint equations for small molecules in molecular dynamics simulations. *J Comput Chem.* 2001;22(5):501–508.
35. Miller BR, McGee TD, Swails JM, Homeyer N, Gohlke H, Roitberg AE. MMPBSA.py: an efficient program for end-state free energy calculations. *J Chem Theor Comput.* 2012;8(9):3314–3321.